Cancer Therapy

International Edition: DOI: 10.1002/anie.201811691
German Edition: DOI: 10.1002/ange.201811691

Molecular Scaffolds as Double-Targeting Agents For the Diagnosis and Treatment of Neuroblastoma

Gonzalo Villaverde, Arantzazu Alfranca, África Gonzalez-Murillo, Gustavo J. Melen, Rafael R. Castillo, Manuel Ramírez, Alejandro Baeza,* and María Vallet-Regí**

Abstract: *The selective delivery of therapeutic and imaging agents to tumoral cells has been postulated as one of the most important challenges in the nanomedicine field. Meta-iodobenzilguanidine (MIBG) is widely used for the diagnosis of neuroblastoma (NB) due to its strong affinity for the norepinephrine transporter (NET), usually overexpressed on the membrane of malignant cells. Herein, a family of novel Y-shaped scaffolds has been synthesized, which have structural analogues of MIBG covalently attached at each end of the Y-structure. The cellular uptake capacity of these double-targeting ligands has been evaluated in vitro and in vivo, yielding one specific Y-shaped structure that is able to be engulfed by the malignant cells, and accumulates in the tumoral tissue, at significantly higher levels than the structure containing only one single targeting agent. This Y-shaped ligand can provide a powerful tool for the current treatment and diagnosis of this disease.*

Neuroblastoma (NB) is the most common extra-cranial solid tumor in childhood. 50% of the cases are diagnosed at late stages when the disease has spread throughout the entire body; the metastatic stage.[1] The treatment of metastatic NB (stage IV) is usually based on the combination of various chemotherapeutic agents in high doses and, in cases of a good response to the initial chemotherapy, the surgical removal of the primary tumor. The treatment is completed with radiotherapy, or the complementation of the initial chemotherapy with an autologous hematopoietic stem cell transplantation and the treatment of possible residual disease with differentiating agents.[2] Despite this multimodal treatment, up to 60% of children with stage IV of NB relapse.[1,2] Thus, the prognosis of advanced NB is very poor, which demonstrates the inability of the current treatment to entirely eradicate the disease. NB cells come from the neural crest, such as precursors of the sympathetic nervous system.[1] Around 95% of NB cells overexpress the transmembrane protein norepinephrine transporter (NET), which is able capture norepinephrine precursors.[3,4,24] The synthetic norepinephrine analogue *meta*-iodobenzylguanidine (MIBG) selectively binds to the NET receptor and for this reason, MIBG labeled with radioactive iodine is widely used for the diagnosis of NB.[5] Several structure–activity relationship (SAR) studies have demonstrated that the benzene ring and the guanidine moiety are required for the NET-binding capacity of MIBG.[5] Thus, the rest of the structure permits some degree of modification, such as the substitution of the iodine for another group with a different electron-donor/ acceptor character. Furthermore, changes in the position of the substitution, and even replacing the aromatic ring itself, have been carried out in an attempt to improve both cell uptake and tumor tissue accumulation.[6–10] However, the in vivo assays did not yield the expected results, with MIBG being found to be the most active. Even the incorporation of a second guanidine group at position 4 led to a significant decrease in the levels of internalization into NB cells.[11] Until now, only the incorporation of a methyl group at position 4 has been found to improve the retention of this molecule by the NB cells.[7–9,11] The MIBG analogue, *meta*-aminobenzylguanidine (MABG), which contains an amino group instead of the iodine, has shown a similar NET-binding ability than that of MIBG.[12] Therefore MABG was conjugated, via organic spacers, to non-radioactive fluorescence compounds, visible in the near infrared, which act as imaging agents,[12] resulting an excellent vectorization agent that yielded improved spatial imaging resolution in comparison to that obtained by single-photon emission computed tomography

[*] Dr. G. Villaverde, Dr. R. R. Castillo, Dr. A. Baeza, Prof. M. Vallet-Regí
Dpto. Química en Ciencias Farmacéuticas. Facultad de Farmacia, Universidad Complutense de Madrid
Plaza Ramon y Cajal s/n. (Spain)
and
Instituto de Investigación Sanitaria Hospital 12 de Octubre i+12 (Spain)
and
Centro de Investigación Biomédica en Red de Bioingeniería, Biomateriales y Nanomedicina (CIBER-BBN)
Madrid (Spain)
E-mail: abaezaga@ucm.es
vallet@ucm.es

Dr. A. Alfranca
Servicio de Inmunología. Hospital Universitario de La Princesa (Spain)
Dr. A. Alfranca, Dr. Á. Gonzalez-Murillo, Dr. G. J. Melen, Dr. M. Ramírez
Instituto de Investigacion Sanitaria La Princesa
Diego de León, 62, 28006 Madrid (Spain)

Dr. Á. Gonzalez-Murillo, Dr. G. J. Melen, Dr. M. Ramírez
Servicio de Hematología y Oncología Pediátrica, Hospital Infantil Universitario Niño Jesús
Madrid (Spain)
E-mail: manuel.ramirez@salud.madrid.org

Dr. A. Baeza
Dpto. Materiales y Producción Aeroespacial, ETSI Aeronáutica y del Espacio, Universidad Politécnica de Madrid
28040 Madrid (Spain)

Supporting information and the ORCID identification number(s) for the author(s) of this article can be found under: https://doi.org/10.1002/anie.201811691.

(SPECT). Furthermore, MABG has been used as a targeting moiety to guide nanoparticles specifically to NB in murine models.[13] MABG was anchored on the surface of mesoporous silica nanoparticles (MSN) via a polyethylene glycol polymer (PEG) of 2000 Da in molecular weight, which acted as spacer between the nanoparticle surface and the recognition moiety. The presence of MABG as a targeting group enhanced the nanoparticle uptake in NB cells by around fourfold. It was also found that the presence of this targeting group on the nanoparticle surface led to the selective accumulation and high retention of the nanocarriers in the tumoral mass of a xenograft mouse model. In contrast, nanoparticles lacking this targeting group were rapidly excreted.[13] This approach was based on the use of a single-targeting agent that interacts with a membrane cell receptor overexpressed in the tumoral cells. Nature usually employs antibodies as recognition agents and these proteins present a Y-shaped structure, able to bind to antigens at two points instead of one.[14] Inspired by these natural molecules, the following two questions were raised: could a synthetic Y-shaped scaffold, which contains two MABG-based binding points, further improve the uptake of a payload by NB cells? And if so, what is the optimal Y-shaped structure that would yield the best NET-binding capacities? This work describes the synthesis and biological evaluation of different Y-shaped scaffolds decorated with MABG analogues, and also with other common targeting moieties, for the development of improved vectorization agents that enable the targeted delivery of therapeutic/ imaging agents to NB.[15] The promising Y-shaped prototype scaffold identified could pave the way for the safer delivery of chemotherapeutic agents to NB cells and also for the more sensitive and efficient diagnosis of NB. Before the construction of Y-shaped moieties, a small collection of MABG-based derivatives was synthesized to enable the selection of the analogue that yielded the highest cellular uptake in NB for the introduction into the Y-shaped scaffold. Different MABG analogues were synthesized, which have halogens attached to the benzyl ring, or with the amide group in *meta* or *para* position. These molecules were then conjugated to a fluorescein-labeled PEG chain of 3500 Da in molecular weight (Figure 1) The PEGylated fluorescein acts as fluorescent marker, which enables their detection in in vitro assays by flow cytometry (fluorescein ($\lambda_{ex} = 492$ nm; $\lambda_{em} = 520$ nm). The fluorescein-labeled single derivatives, F-PEG-S3, (*m*-glycinamido-benzylguanidine), F-PEG-S4 (*p*-glycinamido-benzylguanidine), F-PEG-SCl (*p*-chloro-*m*-glycinamido-benzylguanidine), and F-PEG-SI, (*p*-glycinamido-*m*-iodo-benzylguanidine)) were synthesized from the corresponding compounds with a terminal primary alkyl amine group proportioned by glycine coupling. (Supporting information, Scheme S1–S5). The cellular uptake of these conjugates was evaluated in the NB cell line, NB1691-luc.[25–27] Cells were incubated for 2 hours with each of these conjugates at 50 $\mu g\,mL^{-1}$ in culture medium, washed once with PBS, and then fresh medium was applied. Finally, cells were incubated overnight and then washed with PBS to remove the non-incorporated conjugate. The cellular uptake was measured by flow cytometry, which shows that the introduction of halogens in the benzyl ring yielded a lower internalization capacity, whereas the system that presents only one amide group (both in the *meta* and *para* positions) achieved the best results. After 2 h of incubation with the

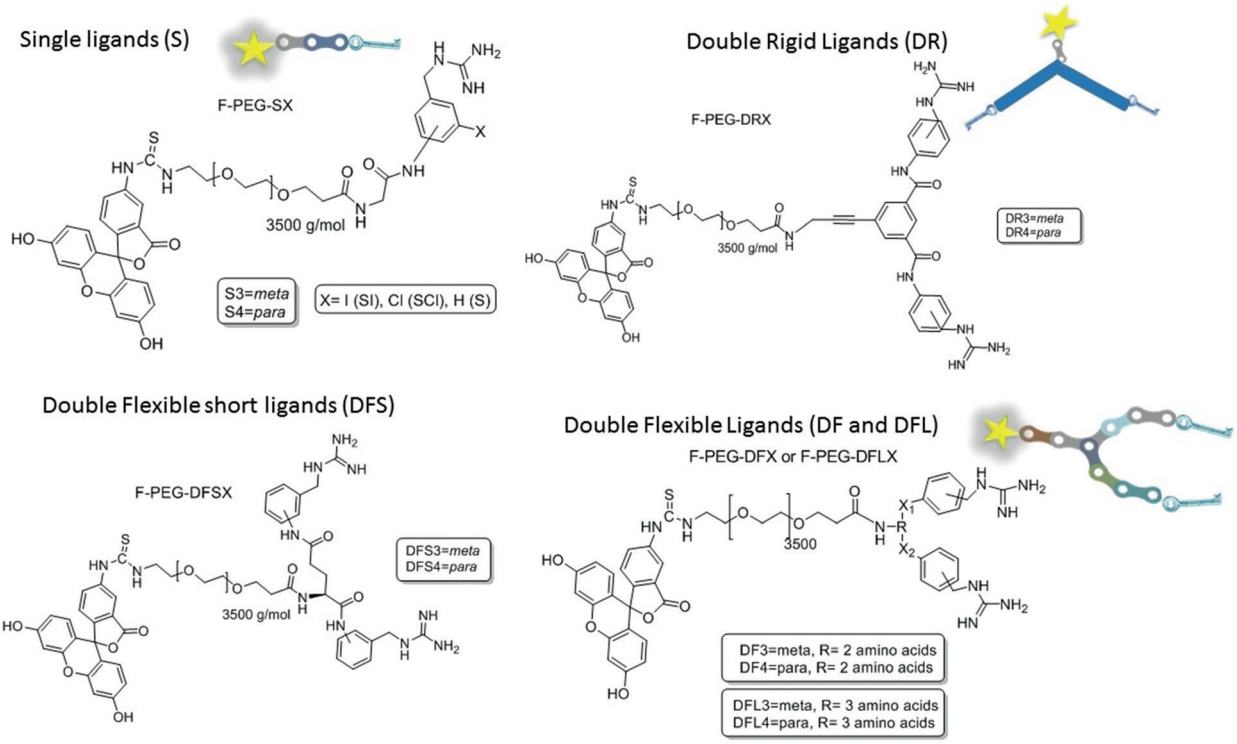

Figure 1. Fluorescein PEGylated analogues for in vitro analysis from all families of single and double-targeting systems. X_1 and X_2 = amide bond in all cases (DF = double flexible; DFL = double flexible large).

corresponding analogue, the *para*-amide substituted compound (S4) showed the best performance with 75% of cells producing fluorescence, versus 50% obtained when using the *meta*-amide (S3). Thus, these *para*- and *meta*-amino derivatives were selected as the best analogues to be incorporated into the Y-shaped structures. As a first attempt at improving the uptake properties of the MAGB analogues, a flexible, medium length Y-shaped scaffold (termed double flexible; DF), composed of two lysines connected by a peptide bond, was chosen as initial candidate to combine the MABG analogues. Other motifs were also tested in combination with the MABG analogues in the DF scaffold. Both targeting agents were connected to the scaffold by amidation of the primary amine groups. For this aim, succinate derivatives of S3 and S4 were synthesized (Supporting Information, Scheme S6) to afford DF3 and DF4. DFS3-TPP and DFS3-RGD were also synthesized. DFS3-TPP was designed with a one lysine peptide scaffold (termed double flexible small; DFS) connecting the succinate S3 analogue and a triphenilphosphine unit, which should selectively target this compound to the mitochondria.[16–18] DFS3-RGD, was constructed with the same structure except the triphenilphosphine unit was exchanged for the tripeptide RGD in an attempt to target two different tumoral receptors that will be present in the NB tumor endothelium and cell membrane.[19] (Supporting Information, Schemes S12 and S13). In all cases the systems have a primary amine group as the exclusive anchoring point to link with the pre-activated acid group of PEG, which is connected to the corresponding payload. Similar to the aforementioned analogues, a fluorescent moiety was anchored to this system for in vitro experiments (F-PEG-DFX). Figure S7 in the Supporting Information shows that more than 90% of cells treated with double systems DF3 and DF4 at 50 $\mu g\,mL^{-1}$, and even at 25 $\mu g\,mL^{-1}$, show fluorescence. 75% of the cells treated with the single-targeting S4 show fluorescence, whereas the rest of the single ligands showed an average of 50% internalization at the higher concentration. The double systems DFS3-TPP and DFS3-RGD showed notable decreases in internalization in comparison to DF3 and DF4, and were even worse than the single agents S3 and S4. This behavior demonstrates that the introduction of nonspecific moieties could interfere with the binding properties of the benzylguanidine group and therefore the recognition by NET. Efforts were then focused on obtaining the best benzylguanidine-based Y-shaped multivalent ligand that could be applied as vectorization agent for NB. For this aim, studies of the influence of the length and flexibility of the scaffold on the uptake properties were carried out for the following F-PEGylated double-ligand families, classified according to their rigid or flexible nature and their length (Figure 1 and Figure 2a); double rigid (DR3 and DR4), double flexible small (DFS3 and DFS4), double flexible (DF3 and DF4), and double flexible large (DFL3 and DFL4).

Double-rigid scaffolds (DR) are based on an aromatic core body. They were synthesized by an amide-formation coupling reaction, using the same starting material described for the single analogues connecting two units of S3 and S4, with a terminal alkyl amine group with an isophthalic acid analogue, for affording the homogeneous DR3 and DR4,

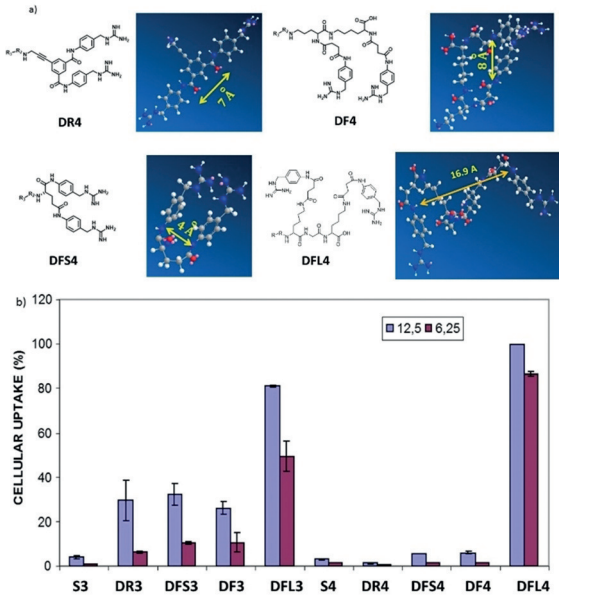

Figure 2. a) Distance, calculated by molecular mechanics (MM2), between recognition spots in the double scaffolds structures DR4 (7 Å), DFS4 (4 Å), DF4 (8 Å), and DFL4 (16.9 Å), NOTE: The distances are equivalent in the case of *meta*-substituted systems. b) Initial screening of single (S3 and S4) versus double ligands for uptake in NB cells at low concentrations, 12.5 $\mu g\,mL^{-1}$ (blue) and 6.25 $\mu g\,mL^{-1}$ (red).

respectively. (Supporting Information, Schemes S7 and S8). Double-flexible scaffolds are based on oligopeptide chains. In this group, three different types of flexible structures were synthesized DFS, DF, and DFL, presenting one, two, and three amino acids, respectively. Briefly, these DF analogues were synthesized by coupling amidebenzylguanidine analogues in *meta* and *para* conformation (S3 and S4) via a peptide chain, affording DFS3 and DFS4 with one amino acid in the structure, DF3 and DF4 with two amino acids, and DFL3 and DFL4 with three amino acids. The increasing length of the amino acid linker confers more flexibility and distance between the binding points. Most of the double-flexible scaffolds group, except the DFS, scaffolds were synthesized using typical solid-phase peptide synthesis, by conventional Fmoc deprotection/HOBT-based acid activation coupling, starting from Fmoc-NH-Lys-NH-Mtt Wang resin. The remaining amino acids, as well as the targeting agents, previously synthesized in this case with terminal carboxylic acid group proportioned by succinic acid coupling with the corresponding initial analogue S3 and S4 (Supporting Information, Schemes S9–11 and Scheme S6), were consecutively coupled. Finally, the complete systems were released from the resin by the addition of TFA cocktail. In vitro experiments for the internalization in NB cells, were carried out by screening the PEGylated and fluorescein-labeled analogues for each family at 12.5 $\mu g\,mL^{-1}$ and 6.5 $\mu g\,mL^{-1}$ following conditions previously described. The analogues analyzed were: S3 and S4, as references, rigid ligands DR3 and DR4, and flexible scaffolds, DFS3, DFS4, DF3, DF4, DFL3, and DFL4.

As Figure 2b shows, the act of doubling the number of targeting moieties did not govern the entire uptake process, but their arrangement, their distance to each other, and their freedom to adopt a cluster configuration in their interaction with the receptor in the cell membrane seemed determinant. Thus, the structure and length of the scaffold have a dominant effect on the interaction with NET on the NB cell membrane. Taking the data for the *meta*-derivative as an example, the double-rigid scaffold DR3 improved the internalization properties to the same extent as the flexible analogue DF3, when compared to its corresponding single counterpart S3. This equal behavior may be explained by the duplication of the interaction points with NET in both analogues. Furthermore, they present an equal distance between recognition points, according to MM2 calculations (DR3 (7 Å), DF7 (8 Å)). Thus, in this case, the effect on the uptake process is governed by the duplication of targeting agent. On the other hand, the larger and more flexible analogue, DFL3 (16 Å distance between recognition points), resulted in the significantly more efficient uptake when compared to S3 and the rest of the ligands in the family. Thus, having two benzylguanidine derivatives in the same system becomes more important when the distance between the recognition moieties increases and the system is flexible.

Para analogues from Figure 2a showed a similar behavior; when the distance between the benzylguanidine analogues was about 16.9 Angstrom (DFL4) the internalization levels increase by around 20-fold versus DR4, DF4, and DFS4. This finding aids understanding of the behavior of the targeting ligand. The distance and the flexibility of the ligand allow the system to work like a common bio-receptor with a double-anchoring point, and if the distant and flexibility of the ligand is not appropriate, the double ligand works as single-targeting agent, interacting via only one of the recognition points present in the scaffold. Thus, comparing the uptake properties of the best bi-functional system (DFL4) with the best mono-functional system (S4), we can conclude that a ten times lower concentration of DFL4 is required for 100% of NB cells to internalize a particular system, when compared to S4. Having characterized the cell uptake properties of these systems, the next step was to study the selective transporting and accumulation of significant payloads (for example, drugs, nanoparticles or imaging agents) to the NB tumoral environment. To achieve this goal, in vivo experiments were conducted to compare ligands with the best performance in vitro (i.e. DFL3 and DFL4) versus a non-targeted system. To this end, MSNs marked with Cy7 were synthesized and surface-functionalized with the corresponding vectorization agents, via a PEG linker chain, affording the control nanoparticle NP-NH_2 and the targeted nanoparticles NP-PEG-DFL3 and NP-PEG-DFL4. Previous results of our group have shown that MSNs are highly efficient nanotransporters for drug

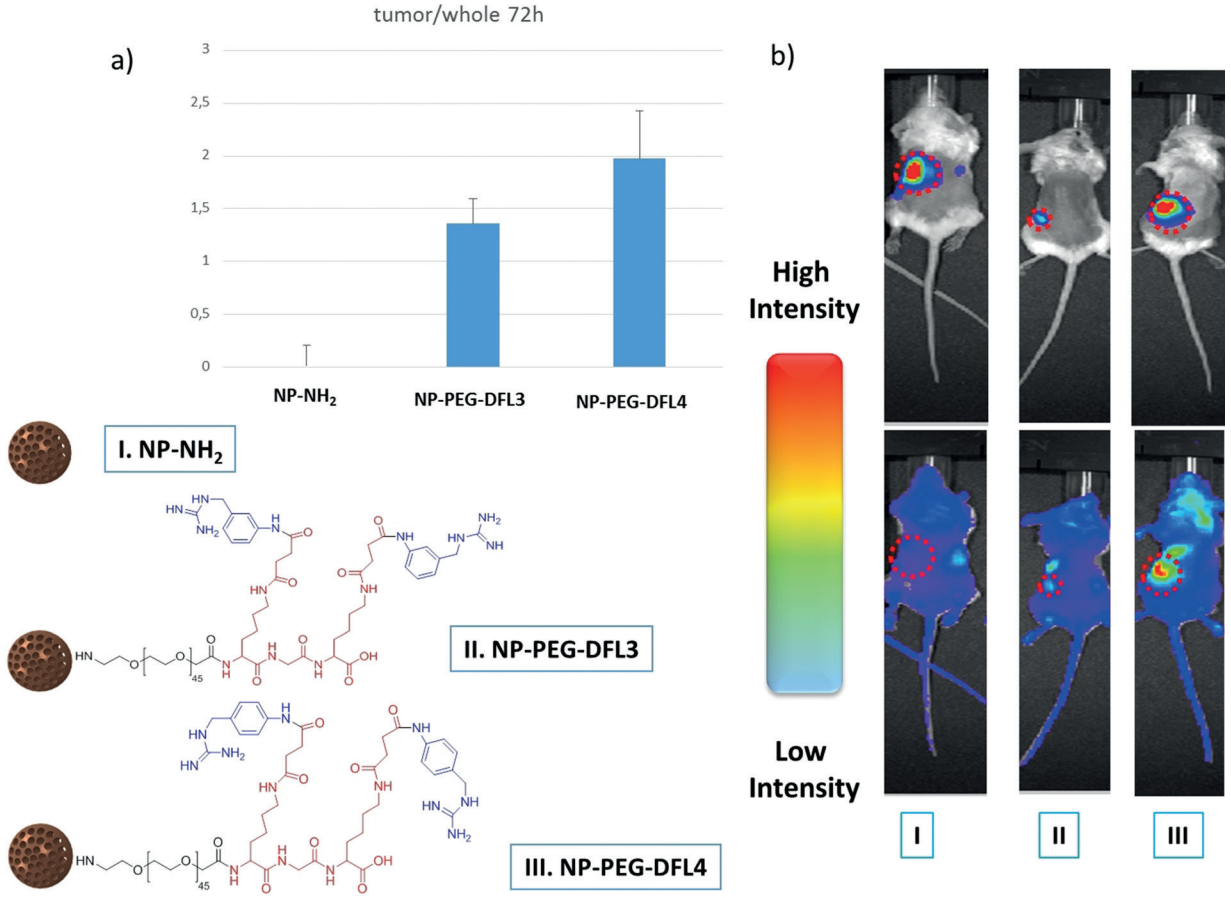

Figure 3. a) Graphic at the top shows relative fluorescent signal (tumor area/whole mouse) obtained from xenograft neuroblastoma-inoculated mice 72 h after injection with either NP-NH2, NP-PEG-DFL3, or NP-PEG-DFL4, shown below, (mean ± SD; $n = 3$–5 per group) b) Representative photographs of xenograft mice treated as in (a), showing luminescent tumor signal (top) and fluorescent nanoparticle signal (bottom).

delivery, due to their optimal loading and controlled release properties. Furthermore, MSNs may be easily functionalized for adding vectorization agents.[20–22] Cy7 is a near infrared marker frequently used for in vivo assays, given the reduced tissue auto fluorescence at this wavelength.[28] This characteristic makes Cy7 a suitable candidate for labeling the nanotransporters for their in vivo evaluation. Functionalization of the agents to the surface of the nanoparticle was carried out via a PEG linker; PEG confers more ability in dispersion and helps to abolish the opsonization process which may prolong circulation time in the blood stream.[23] Human neuroblastoma NB1691-luc cells (2×10^6 cells/mouse) were subcutaneously implanted into the flank of immunodeficient NGS mice (NOD/SCID deficient in the common gamma chain). These cells constitutively express luciferase, which allows the in vivo monitoring of tumor growth by bioluminescence quantification upon injection of the luciferase substrate luciferin (1.25 mg/mouse). Three weeks after cell inoculation, tumor development in mice was assessed, and mice were sorted into three groups with a homogeneous distribution of tumor size among them (3–5 specimens per group; Supporting Information, Figures S9 and S10). Mice received intravenous injections of 1 mg of NP-NH_2, NP-PEG-DFL3, or NP-PEG-DFL4 in 0.2 mL of saline solution. To evaluate system accumulation in the tumor mass in each case, the fluorescent signal ratio of Cy7 was quantified in the tumor area vs. the whole mouse, at 72 hours after system administration. As shown in Figure 3, the preferential accumulation of targeted MSN systems (NP-PEG-DFL3 and NP-PEG-DFL4) was observed in tumor mass, which was detected by bioluminescence. In conclusion, this work has allowed the selection of a novel system based on a Y-shaped multivalent double-ligand targeting agent for NB with a specific composition and length. Their behavior in terms of selectivity and efficacy for improving cell internalization and in vivo accumulation in NB xenografts has been evaluated. This new Y-shaped double system presents a substantial improvement in cell uptake in vitro, 20-times higher than the single-targeted system and an effective accumulation in tumor mass in vivo. Furthermore, they are easily tunable for use as versatile targeting system for drug delivery in conjugates or nano-transporters, as well as for imaging agents. Our findings may pave the way for increasing the efficacy of diagnosis and treatment of NB.

Acknowledgements

M.V.R. thanks the European Research Council for funding through the Advanced Grant VERDI (ERC-2015 AdG proposal no. 694160) and Asociación NEN. Financial support from Ministerio de Economía *y* Competitividad, (MEC), Spain (Project MAT2015-64831-R) is gratefully acknowledged. A.A. is supported by grant FIS PI15/01491. M.R. is supported by Asociación NEN, Asociación Pablo Ugarte and Fundación Neuroblastoma.

Conflict of interest

The authors declare no conflict of interest.

Keywords: *meta*-iodobenzylguanidine · molecular scaffold · nanomedicine · neuroblastoma · targeting

How to cite: *Angew. Chem. Int. Ed.* **2019**, *58*, 3067–3072
Angew. Chem. **2019**, *131*, 3099–3104

[1] J. M. Maris, *N. Engl. J. Med.* **2010**, *362*, 2202–2211.
[2] N. R. Pinto, M. A. Applebaum, S. L. Volchenboum, K. K. Matthay, W. B. London, P. F. Ambros, A. Nakagawara, F. Berthold, G. Schleiermacher, J. R. Park, D. Valteau-Couanet, A. D Pearson, S. L. Cohn, *J. Clin. Oncol.* **2015**, *33*, 3008–3017.
[3] S. Carlin, R. J. Mairs, A. G. Mccluskey, D. A. Tweddle, A. Sprigg, C. Estlin, J. Board, R. E. George, C. Ellershaw, A. D. Pearson, J. Lunec, P. G. Montaldo, M. Ponzoni, B. L. van Eck-Smit, C. A. Hoefnagel, M. D. van den Brug, G. A. Tytgat, H. N. Caron, *Clin. Cancer Res.* **2003**, *9*, 3338–3344.
[4] K. K. Matthay, R. E. George, A. L. Yu, *Clin. Cancer Res.* **2012**, *18*, 2740–2753.
[5] A. Schlessinger, E. Geier, H. Fan, J. J. Irwin, B. K. Shoichet, K. M. Giacomini, A. Sali, *Proc. Natl. Acad. Sci. USA* **2011**, *108*, 15810–15815.
[6] D. Hadrich, F. Berthold, E. Steckhan, H. Bönisch, *J. Med. Chem.* **1999**, *42*, 3101–3108.
[7] G. Vaidyanathan, S. Shankar, D. J. Affleck, P. C. Welsh, S. K. Slade, M. R. Zalutsky, *Bioconjug. Chem.* **2001**, 798–806.
[8] G. Vaidyanathan, S. Shankar, M. R. Zalutsky, *Bioconjug. Chem.* **2001**, 786–797.
[9] G. Vaidyanathan, P. C. Welsh, K. C. Vitorello, S. Snyder, H. S. Friedman, M. R. Zalutsky, *Eur. J. Nucl. Med. Mol. Imaging* **2004**, *31*, 1362–1370.
[10] K. A. Streby, N. Shah, M. A. Ranalli, A. Kunkler, T. P. Cripe, *Pediatr. Blood Cancer* **2015**, *62*, 5–11.
[11] G. Vaidyanathan, S. Shankar, D. J. Affleck, K. Alston, J. Norman, P. Welsh, H. LeGrand, M. R. Zalutsky, *Bioorg. Med. Chem.* **2004**, *12*, 1649–1656.
[12] W. Wang, J. Shohet, M. Mawad, S. Ke, *Non-Radioactive Agents for Neuroblastoma Imaging*, WO/2011/123742,USA **2011**.
[13] G. Villaverde, A. Baeza, G. J. Melen, A. Alfranca, M. Ramirez, M. Vallet-Regí, *J. Mater. Chem. B* **2015**, *3*, 4831–4842.
[14] T. Quynh, N. Nguyen, K. W. Lim, A. T. Phan, *Sci. Rep* **2017**, *33*, 1–7.
[15] V. J. Yao, S. D. Angelo, K. S. Butler, C. Theron, T. L. Smith, S. Marchiò, J. G. Gelovani, R. L. Sidman, A. S. Dobroff, C. J. Brinker, et al., *J. Controlled Release* **2016**, *240*, 267–286.
[16] G.-F. Luo, W.-H. Chen, Y. Liu, Q. Lei, R.-X. Zhuo, X.-Z. Zhang, *Sci. Rep.* **2014**, *4*, 1–10.
[17] B. H. Kang, J. Plescia, H. Y. Song, M. Meli, G. Colombo, K. Beebe, B. Scroggins, L. Neckers, D. C. Altieri, *J. Clin. Invest.* **2009**, *119*, 454–464.
[18] W.-H. Chen, X.-D. Xu, G.-F. Luo, H.-Z. Jia, Q. Lei, S.-X. Cheng, R.-X. Zhuo, X.-Z. Zhang, *Sci. Rep.* **2013**, *3*, 3468.
[19] E. V Rosca, J. M. Stukel, R. J. Gillies, J. Vagner, M. R. Caplan, *Biomacromolecules* **2007**, 3830–3835.
[20] M. Vallet-Regi, A. Rámila, R. P. del Real, J. Pérez-Pariente, *Chem. Mater.* **2001**, *13*, 308–311.
[21] M. Vallet-Regí, E. Ruiz-Hernández, *Adv. Mater.* **2011**, *23*, 5177–5218.
[22] A. Baeza, M. Colilla, M. Vallet-Regí, *Expert Opin. Drug Delivery* **2014**, 1–19.
[23] H. Meng, M. Liong, T. Xia, Z. Li, Z. Ji, J. I. Zink, A. E. Nel, *ACS Nano* **2010**, *4*, 4539–4550.

[24] K. A. Streby, N. Shah, M. A. Ranalli, A. Kunkler, T. P. Cripe, *Pediatr. Blood Cancer* **2015**, *62*, 5 – 11.
[25] J. L. Harenza, M. A. Diamond, R. N. Adams, M. M. Song, H. L. Davidson, L. S. Hart, M. H. Dent, P. Fortina, C. P. Reynolds, J. M. Maris, *Sci. Data* **2017**, *4*, 170033.
[26] J. Thompson, W. C. Zamboni, P. J. Cheshire, L. Lutz, X. Luo, Y. Li, J. A. Houghton, C. F. Stewart, P. J. Houghton *Clin. Cancer Res.* **1997**, 423 – 431.
[27] A. Tivnan, W. S. Orr, V. Gubala, R. Nooney, D. E. Williams, C. McDonagh, S. Prenter, H. Harvey, R. Domingo-Fernández, I. M. Bray, O. Piskareva, N. G. CY, H. N. Lode, A. M. Davidoff, R. L. Stallings, PLoS One 2012, 7, e38129.
[28] R. Hernandez, S. Heskamp, M. Rijpkema, D. L. Bos, D. M. Goldenberg, W. J. McBride, A. Morgenstern, F. Bruchertseifer, W. Cai, O. C. Boerman, *Theranostics* **2017**, *7*, 1—8.

Manuscript received: October 11, 2018
Revised manuscript received: November 30, 2018
Accepted manuscript online: December 10, 2018
Version of record online: January 9, 2019

